2012

Rigorous Characterization of Carbon Nanotube Complex Permittivity over a Broadband of RF Frequencies

Emmanuel Decrossas

Mahmoud EL Sabbagh
Syracuse University, msabbagh@syr.edu

Victor Fouad Hanna

Samir M. El-Ghazaly

Recommended Citation

E. Decrossas, M. A. El Sabbagh, V. F. Hanna, and S. M. El-Ghazaly, "Rigorous Characterization of Carbon Nanotube Complex Permittivity Over a Broadband of RF Frequencies," Ieee Transactions on Electromagnetic Compatibility, vol. 54, pp. 81-87, Feb 2012.

Rigorous Characterization of Carbon Nanotube Complex Permittivity over a Broadband of RF Frequencies

E. Decrossas, *Student Member, IEEE,* M. A. EL Sabbagh, *Senior Member, IEEE*, V. Fouad Hanna, *Fellow, IEEE,* and S. M. El-Ghazaly, *Fellow, IEEE*

***Abstract*—This work presents a comprehensive characterization of the frequency dependence of the effective complex permittivity of bundled carbon nanotubes considering different densities over a broadband of frequencies from 10 MHz to 50 GHz using only one measurement setup. The extraction technique is based on rigorous modeling of coaxial and circular discontinuities using mode matching technique in conjunction with inverse optimization method to map the simulated scattering parameters to those measured by vector network analyzer. The dramatic values of complex permittivity obtained at low frequencies are physically explained by the percolation theory. The effective permittivity of a mixture of nano-particles of alumina and carbon nanotubes versus frequency and packing density is studied to verify the previously obtained phenomenon.**

***Index terms*—Alumina, broadband, carbon nanotubes, coaxial discontinuities, complex permittivity measurements, mode matching technique, nano-particles, radio frequency.**

I. Introduction

SINCE its discovery in 1991 by S. Iijima [1], carbon nanotubes (CNTs) have attracted strong interests. CNTs present a very high tensile strength, thermal conductivity, and high electrical conductivity due to the strong carbon-carbon covalent bonding. Many applications have been investigated such as radio frequency (RF) resonators, field-effect transistors, chemical and mechanical sensors [2]-[4]. Usually, CNTs are classified into two categories: single-walled CNTs (SWCNT) composed of a single graphitic cylinder where the diameter varies from 0.7 to 2 nm and multi-walled CNTs (MWCNTs) composed of several concentric graphitic layers where the diameter varies from 10 to 200 nm [4]. The knowledge of the electrical properties of CNTs over a broadband of frequencies is necessary to implement novel RF/microwave carbon nanotubes based devices. Different material characterization techniques used to extract complex permittivity are presented in [5]. Nevertheless, the electrical characterization of carbon nanotube networks can be challenging because it usually requires special preparation of either a thin film or embedding CNTs into a host medium which decreases the accuracy of extracted complex permittivity. The effects of a sample preparation are difficult to characterize which explains the variations of the extracted permittivity previously reported in [6]-[7]. EL Sabbagh *et al.* present a technique of extraction based on planar transmission line measurements where the metallic trace of the transmission line is replaced by CNT networks [8]. Nevertheless, in this technique, the maximum measurement frequency is limited to 400 MHz due to the restriction that only the fundamental mode propagates in the structure.

There are several advantages of the method used in this work: no special preparation is necessary; only a small fraction of material under test (MUT) is used; MUT can be solid, granular, or liquid; low cost; non-destructive; easily implemented; and only a single test structure is used to cover a broadband of frequencies from 10 MHz to 50 GHz [9]. The CNT networks as furnished by the supplier without any further processing is directly deposited in a hollow circular waveguide shorted at its end and connected at the other end to a vector network analyzer (VNA) via a coaxial precision adapter. A similar permittivity extraction procedure has been studied in [10] where coaxial discontinuities are characterized based on the computation of the input admittance of dominant mode including contributions from higher-order modes. In this work instead, the discontinuities encountered by an incident wave are characterized by computing their generalized scattering matrices (GSMs) based on the mode matching [11] technique (MMT) to obtain the generalized input reflection coefficient S_{11} which is directly measurable by VNA. The accuracy of the discontinuity model is insured by considering all higher-order modes both propagating and evanescent in the different region of the setup shown in Fig. 1. The reflection coefficients obtained from MMT and measurements are compared. Knowing the complex permittivity of the MUT, the computation of the input reflection coefficient is straightforward. On the other hand, to extract complex permittivity from comparison between computed and measured reflection coefficients, an iterative first-order gradient optimization method is implemented. The analytical mode matching formulation used to extract the complex permittivity of any MUT over a broadband of radio frequencies (RF) was introduced in [12]. Detailed

Manuscript received XX XX, 2011.
This work was supported by the Army Research Laboratory.

Emmanuel Decrossas is with the Dept. of Electrical Engineering, University of Arkansas, Fayetteville, AR, 72701, USA. (e-mail: edecrossas@ieee.org).

Mahmoud A. EL Sabbagh is with the Dept. of Electrical Engineering and Computer Science, University of Syracuse, Syracuse, NY, 13244, USA. (e-mail: msabbagh@ieee.org).

Victor Fouad Hanna is with the Université Pierre et Marie Curie - Paris 6, EA 2385, L2E, F-75252, Paris, France. (e-mail:victor.fouad_hanna@upmc.fr).

Samir M. El-Ghazaly is with the Dept. of Electrical Engineering, University of Arkansas, Fayetteville, AR, 72701, USA. (e-mail: elghazal@uark.edu).

convergence studies were presented to find the appropriate number of modes to rigorously characterize each discontinuity in the setup. Details about the inverse gradient approach used to find complex permittivity is included in Appendix at the end of paper. The validity of modeling was verified by comparison with other numerical technique such as Finite Element Method (FEM). The results presented in [12] show the superiority of MMT over FEM considering the structure shown in Fig. 1. Moreover, the procedure was applied to air as lossless material and to distilled water as lossy material where the results were compared with available data in the literature. Section II describes the actual test setup used in this work. Section III presents the extracted effective complex permittivity results for pure CNTs networks in its dry form as furnished by the supplier. The large values of the effective permittivity are physically explained based on the percolation theory and demonstrated by studying the complex effective permittivity variation with packing density and frequency. Moreover, the characterization of CNT networks mixed with nano-particles of alumina is studied and the results show the enhancement of effective permittivity versus packing density.

II. Description of Test Setup

The test setup described in Fig. 1 consists of a hollow circular waveguide connected to a coaxial waveguide. The structure has been designed to be connected directly to the coaxial cable of a performance network analyzer (PNA): Agilent E8361A via a 1.85 mm to 2.4 mm precision adapter. The advantage of this test structure is that the calibration plane is in direct contact with the material under test avoiding any phase ambiguity in the measurements of the reflection coefficient [13].

For modeling purposes, the testing setup is divided into three main regions. Region I is the 2.4 mm male part of the adapter, modeled as a 50-Ω coaxial line. The other side of the adapter not presented here is a 1.85 mm female attached to a 1.85 mm male coaxial cable connected to the PNA on the other end. Region II represents the pin of the 2.4 mm male side of the adapter going inside the cell. These regions are modeled as coaxial transmission lines filled with different dielectric medium. Region III is the circular waveguide terminated by a short circuit. Regions II and III define the broadband circular waveguide holder where the MUT is inserted. The full-wave model based on the MMT depicted in Fig. 1 has been rigorously described in [12]. Fig. 2 shows the actual testing device which is made of soft copper material.

III. Experimental Results and Discussion

For the purpose of accurate measurements over a broadband of frequencies, the calibration of the PNA is carried out over three different frequency ranges: first range from 10 MHz to 1 GHz, second range from 1 GHz to 20 GHz, and last range from 20 GHz to 50 GHz. In each frequency range, the short, open, load, and thru (SOLT) calibration is adopted. 201 frequency points are considered in each frequency range. The intermediate frequency (IF) bandwidth is set to 70 Hz which increases the dynamic range of analyzer; reduces noise; and minimizes calibration errors.

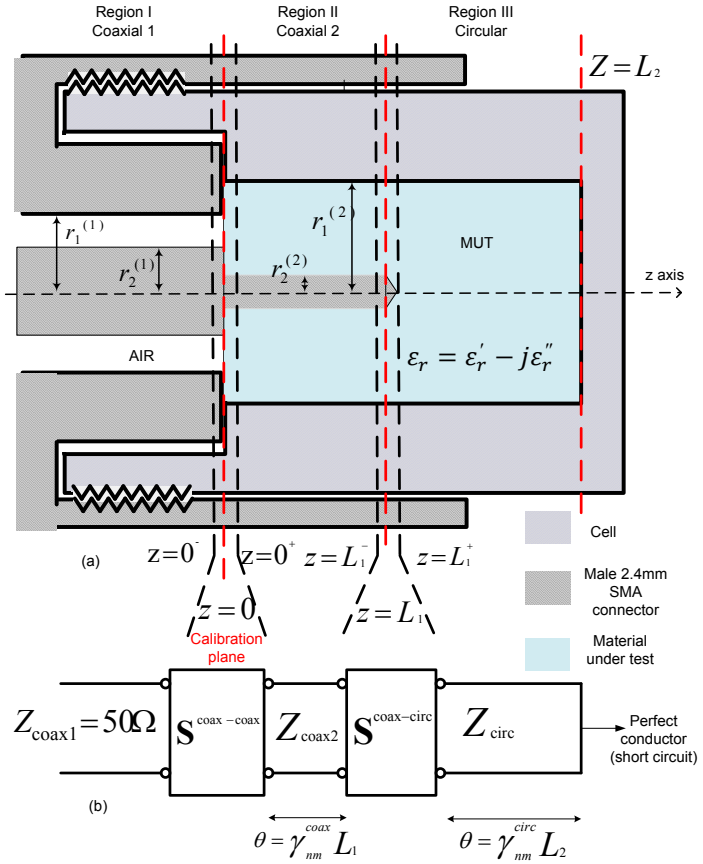

Fig. 1. (a) The schematic of test setup. (b) Generalized scattering matrices building blocks. Dimensions of design parameters are: $r_1^{(1)}$ = 1.2 mm, $r_2^{(1)}$ = 0.52 mm, $r_1^{(2)}$ = 1.26 mm, $r_2^{(2)}$ = 0.254 mm, L_1 = 1.1 mm, L_2 = 5.3 mm.

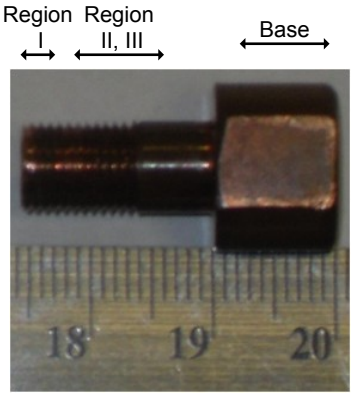

Fig. 2: Actual picture of the fabricated testing structures. Regions I, II, and III are the same as those shown in the schematic of Fig. 1.

The extraction technique proposed in this work has been successfully validated for the characterization of water as a lossy material and the characterization of air as a lossless material at room temperature [9] and [12].

A. Complex Permittivity of Carbon Nanotubes

In this part of study, bundled networks of single-walled CNTs are used as provided by manufacturer (Sigma-Aldrich):

the sample purity is 50 to 70 volume percentage as determined by Raman spectroscopy and scanning electron microscopy (SEM) which shows that the sample contains residual catalyst impurities of nickel and yttrium. The length of an individual CNT is approximately 20 μm. Several images are taken by SEM and they reveal the presence of multi-walled CNTs as well as single-walled CNTs within the sample which is in agreement with similar measurements reported in [14].

Fig. 3–Fig. 6 present the variation of the real and imaginary parts of the relative complex permittivity ($\varepsilon_r = \varepsilon_r' - j\varepsilon_r''$) over a broadband from 10 MHz to 50 GHz corresponding to different packing densities of CNTs. Packing density is computed using the relation:

$$\rho = \frac{M}{V}\ (\mathrm{g/cm^3})$$

where M is the mass of MUT in grams weighed using an **analytical balance** and V is the volume of cavity in $\mathrm{cm^3}$ determined through optical measurements.

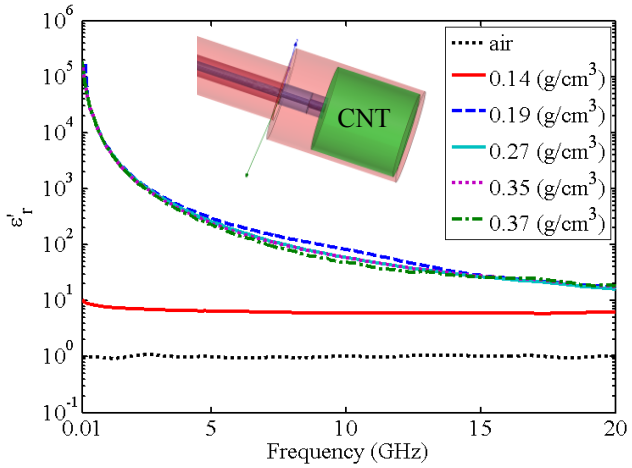

Fig. 3: Variation of the real part of the relative complex permittivity of CNT networks in the frequency range 10 MHz to 20 GHz for different packing densities. The y-axis is in logarithmic scale to show the dramatic variation of the real part of the permittivity. Permittivity of air is included for reference.

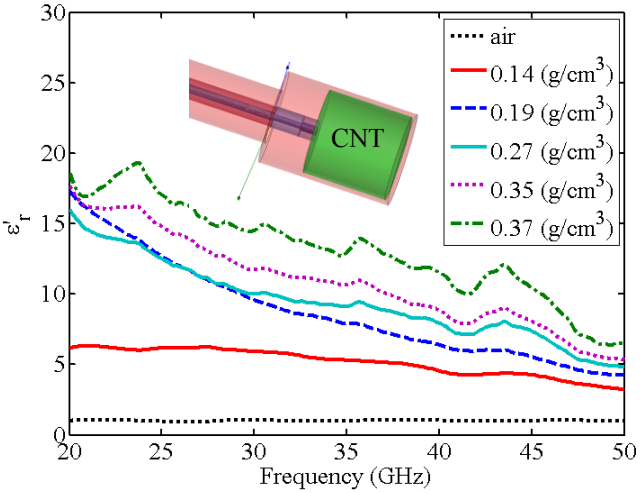

Fig. 4: Variation of the real part of the permittivity of CNT networks in the frequency range 20 GHz to 50 GHz for different packing densities. The linear vertical scale indicates a small variation of the real of the permittivity, suggesting asymptotic values. Permittivity of air is included for reference.

The plots are divided into two frequency bands to highlight the different trends of permittivity at the lower and the upper ends of measurement frequency range. The graphs given in Fig. 3 and Fig. 4 indicate that the highest value of the real part of the relative complex permittivity obtained at 10 MHz is 1.6×10^5 and decreases continuously to finally reach 6.5 at 50 GHz. Similarly, the highest value of the imaginary part of the relative complex permittivity at 10 MHz is 4.1×10^3 as shown in Fig. 5 and decreases to 7 at 50 GHz as shown in Fig. 6. The values of complex permittivity obtained at high frequencies are in agreement with those values reported in [15]. Moreover, the large values at low frequencies are consistent with those large values reported in [14] and [16].

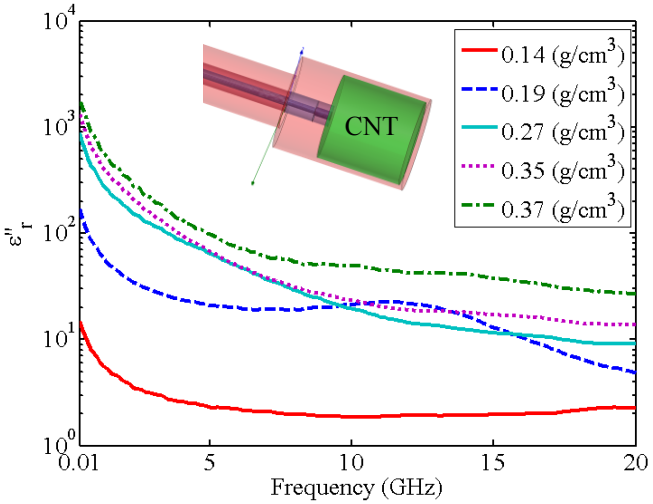

Fig. 5: Variation of the imaginary part of the relative permittivity of CNT networks in the frequency range 10 MHz to 20 GHz for different packing densities. The y-axis is in logarithmic scale to show the dramatic variation of the imaginary part of the permittivity. The imaginary part of the permittivity for air is not plotted in log scale because it is less than 10^{-3} which is outside the range of interest.

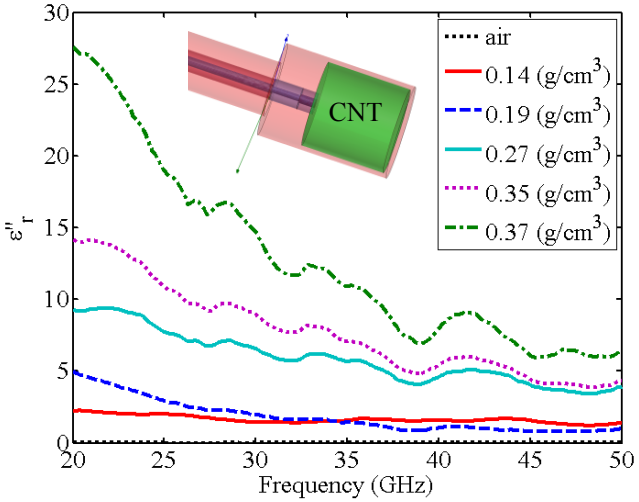

Fig. 6: Variation of the imaginary part of the permittivity of CNT networks in the frequency range 20 GHz to 50 GHz for different packing densities. The linear scale indicates a small variation of the imaginary part of the permittivity, suggesting asymptotic values.

The experimental results show an enhancement of complex permittivity with packing density. At low frequencies, the high values of relative effective permittivity can be attributed to the conductivity of carbon nanotubes as reported in [16]. These high values are consistent with the percolation behavior [17] of the mixture of metallic and semiconducting carbon nanotubes [18]. In other words, a percolation threshold frequency marks the onset of material changing behavior. Below this frequency, the material has dramatic values of effective complex permittivity. Above this frequency, the complex permittivity asymptotically saturates toward the expected value of permittivity for bulk material. It is noted that without any post processing after their manufacture, CNTs consist of a mixture of conducting and semiconducting nanotubes with a ratio of 1:2 depending on their chirality, i.e., 1/3 metallic tubes are mixed with 2/3 of semiconducting nanotubes. Fluctuations in the extracted values of dielectric properties especially at higher frequencies may be attributed to the random nature of CNT networks which includes randomness in number of semiconducting and conducting nanotubes, the randomness of orientation and alignment of nanotubes. To avoid this effect, statistical measurement variations are to be considered to get smooth results. Another reason is the assumption virtually considered in any modeling technique that surface roughness is neglected. This has quite a strong effect on the extracted dielectric constant as frequency goes up explaining why the fluctuations occur at the same frequencies independently of the packing density. A measurement scenario without CNTs which corresponds to air is included for reference purposes. This case was originally presented in [12] and added here to serve as a reference in Figs. 3, 4, and 6. We observe quite a constant value of dielectric constant as a function of frequency when the packing density of CNTs is little as it is dominated by air.

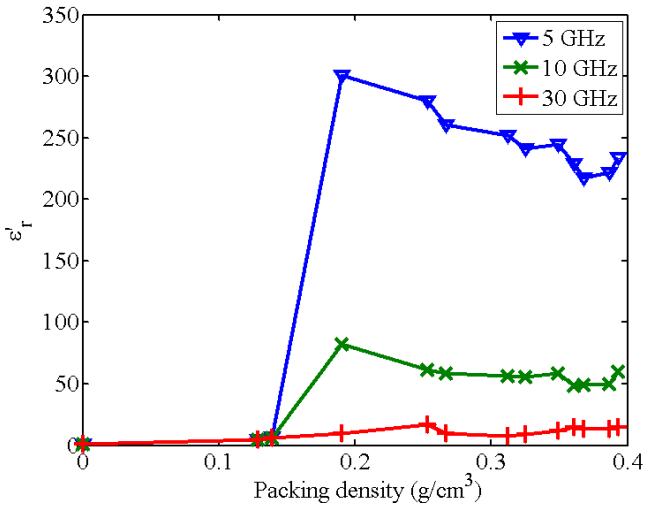

Fig. 7: Variation of the real part of the effective permittivity of CNT networks as a function of packing density at 5, 10 and 30 GHz.

Above a packing density of 0.15 g/cm^3, we observe a percolation behavior of permittivity versus density of CNTs as shown in Fig. 7 due to the dramatic increase of number of nanotubes and the reduction of air interstices. The data in Fig. 7 and Fig. 8 are obtained from results shown in Figs. 3, 4, 5 and 6 at 5, 10 and 30 GHz as well other measurements with different packing densities. The results in Fig. 7 indicate a percolation behavior which is quite significant for lower frequencies, e.g., 5 GHz. After the percolation threshold, the dielectric constant decreases as the packing density increases. The same behavior also occurs at higher test frequencies such as 10 and 30 GHz yet with slower variation of dielectric constant. These results are in agreement with those in Fig. 3 where it is shown that in the frequency range from 5 GHz to 15 GHz, the dielectric constant corresponding to the highest

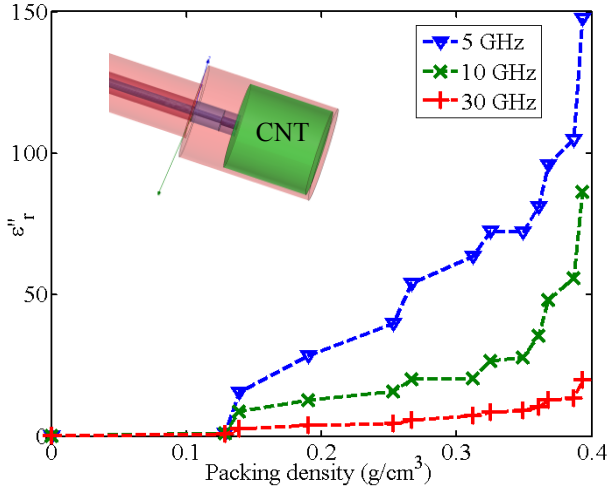

Fig. 8: Variation of the imaginary part of the relative permittivity of CNT networks as a function of packing density at 5, 10 and 30 GHz.

packing density is lower than the dielectric constant corresponding to intermediate densities. This effect is less prominent as the frequency goes higher. It is noted that while the dielectric constant is decreasing with packing density, the imaginary part is increasing as the packing density goes beyond the percolation threshold density $\rho = 0.15$ g/cm^3 as shown in Fig. 8. Below this percolation threshold density, metallic CNTs are separated by semiconducting ones. As the packing density increases, the spacing between conducting CNTs becomes smaller creating nano-capacitors which significantly increases the real part of the effective permittivity until it reaches a peak value exactly at the percolation threshold density [19]. In other words, above the percolation threshold density, connected conductive paths are completely formed in the material which leads to the dramatic increase of losses ($\varepsilon''_r = \frac{\sigma}{\omega}$ where σ is the conductivity of the MUT and ω is the angular frequency) at a packing density of 0.4 g/cm^3. Above the percolation threshold density, the effective real part of permittivity decreases since relative dielectric constant of a metallic material is unity.

B. Effective permittivity of carbon nanotubes mixed with nano particles of alumina

In this part of study, single-walled CNTs are mixed with nano-particles of pure alumina. The alumina used in this work is supplied by South Bay Technology, Inc. The nano particles of alumina have a diameter of 50 nm. The CNTs are used as provided by Bucky USA (product number BU-203) and they

have a purity > 90 wt%, ash < 1.5 wt%, diameter 1 nm to 2 nm, and length 5 μm to 30 μm. Fig. 9 is an image obtained by scanning electron microscopy (SEM) of the mixture of 1 g alumina and 0.2 g CNTs.

The real part of the effective permittivity of a mixture of 0.2 g CNTs and 1 g of nano particles of pure versus frequency is presented in Fig. 10 considering different packing densities of the mixture. For a low packing density, the effective permittivity of the mixture is low as it is dominated by air.

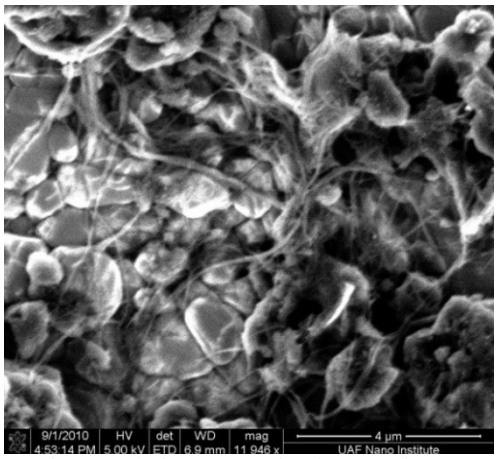

Fig. 9: SEM picture of the prepared mixture of 0.2 g carbon nanotubes mixed with 1 g alumina powder.

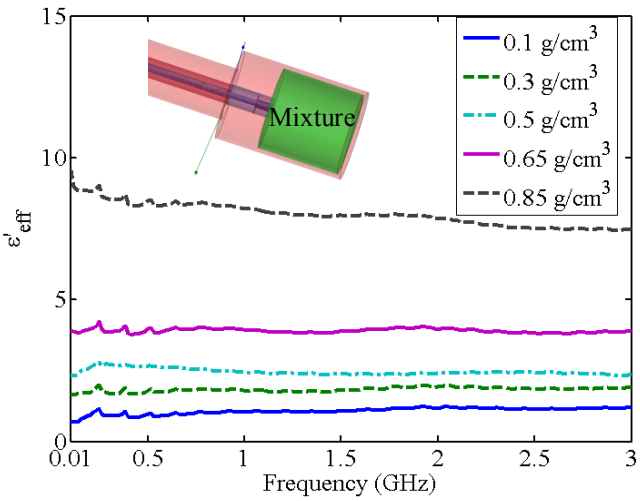

Fig. 10: Variation of the real part of the effective permittivity of a mixture of 0.2 g CNTs and 1 g of nano particles of pure alumina versus frequency using the test setup shown in the inset.

As the packing density increases, air interstices between particles are reduced and a sharp increase of the effective permittivity is observed due to the effective presence of CNTs mixed with alumina.

Fig. 11 shows a comparison between the real part of the effective permittivity of alumina mixed with CNTs and pure alumina to highlight the role of CNTs in the enhancement of the real part of the effective permittivity as the packing density increases. The results of alumina mixture with those CNT networks were measured at 60 MHz as we anticipate the most significant effect of CNTs on the mixture. The results in Fig. 11 verify the high values of permittivity of CNTs shown in Fig. 3. As frequency goes higher, we do not expect that CNTs have that comparable strong effect on permittivity as at low frequencies. Looking closely to Fig. 10, we observe that the variation of the dielectric constant at low frequencies is higher than at high frequencies for any packing density. The linear increase of permittivity of pure alumina versus packing density is due to addition of more material which replaces air and hence permittivity is increasing. It is noted that the value of dielectric constant for bulk alumina depends on the density of alumina. For example, CoorsTek reports a dielectric constant varying from 8.2 to 9.8 corresponding to Alumina density varying from 3.42 to 3.92, respectively. Ultimately, if we could reach an ultimate packing density of alumina close to 3.92 g/cm^3, then we expect to have a dielectric constant equal to 9.8. The linear trend of permittivity is based on measurements and studies presented in [18] for the same material.

It is noted that the percolation behavior is enhanced due to the specific shape of nanotubes, the size of nano metallic particles. The cylindrical shapes of CNTs increase considerably the number of interconnection while the nanosize improves the dispersion in the medium.

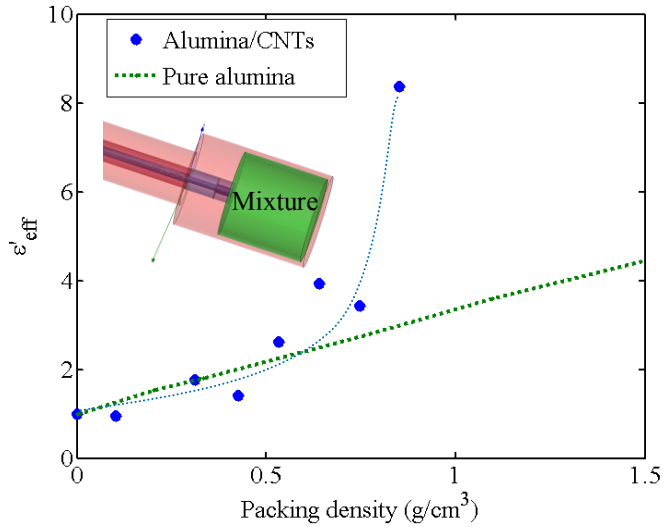

Fig. 11: Variation of the real part of the effective permittivity of a mixture of 0.2 g CNTs and 1 g pure alumina versus packing density realized at 60 MHz. The variation of the real part of the effective permittivity [18] for the same pure alumina versus packing density illustrates enhancement effect due to the addition of CNTs.

Link *et al.* in [20] reported the importance of the aspect ratio with respect to the variation of the dielectric constant for gold nanorods and the effect on the dielectric constant of medium.

IV. Conclusions

A non-destructive, low-cost, easily implemented technique where only a small fraction of material is needed is presented to characterize carbon nanotube based materials in powder form over a broadband of RF frequencies. Only a single measurement setup is required to achieve characterization over the broadband of frequencies from 10 MHz to 50 GHz.

Effective permittivity has been successfully obtained using an optimized gradient method by matching the simulated and measured reflection coefficients. Finally, the frequency dependence of effective complex permittivity and the effects of the packing density of CNTs networks are presented. The complex permittivity obtained for a mixture of carbon nanotubes with nano-particles of alumina suggest the possibility to dramatically increase the effective permittivity for the purpose of engineering novel composite materials.

ACKNOWLEDGMENT

The authors thank H.A. Naseem for useful conversations on this topic, D. Rogers for the fabrication of the test structure and M. Benamara for his fruitful advices about the preparation of SEM samples. Research was sponsored by the Army Research Laboratory and was accomplished under Cooperative Agreement Number W911NF-10-2-0072. The views and conclusions contained in this document are those of the authors and should not be interpreted as representing the official policies, either expressed or implied, of the Army Research Laboratory or the U.S. Government. The U.S. Government is authorized to reproduce and distribute reprints for Government purposes notwithstanding any copyright notation herein.

APPENDIX

Inverse gradient method

The complex permittivity is extracted by using an optimized first order gradient method. The scattering parameters are computed using the mode matching method and compared to the measured reflection coefficient. The complex permittivity $(\varepsilon_r = \varepsilon_r' - j\varepsilon_r'')$ is converted in initial vector form:

$$\hat{a}_0 = \begin{bmatrix} \varepsilon' \\ \varepsilon'' \end{bmatrix} \quad (1)$$

Then an error vector is defined to evaluate the difference between the measured and simulated S-parameters S_{11}.

$$\Delta\vec{S} = \begin{bmatrix} S_{11x}^{(m)} - S_{11x}^{(c)} \\ S_{11y}^{(m)} - S_{11y}^{(c)} \end{bmatrix} \quad (2)$$

where *m* and *c* denote the measured and calculated S-parameters in rectangular coordinates. The error vector is associated to the complex permittivity vector via the derivative matrix as:

$$\Delta\vec{S} = \begin{bmatrix} \frac{\partial S_{11x}}{\partial \varepsilon'} & \frac{\partial S_{11x}}{\partial \varepsilon''} \\ \frac{\partial S_{11y}}{\partial \varepsilon'} & \frac{\partial S_{11y}}{\partial \varepsilon''} \end{bmatrix} \begin{bmatrix} \Delta\varepsilon' \\ \Delta\varepsilon'' \end{bmatrix} \quad (3)$$

The new values of the real and imaginary part of the permittivity are found by inversing the derivative matrix while the new search direction is given by:

$$\hat{a}_n = \hat{a}_{n-1} + \begin{bmatrix} \propto_1 \Delta\varepsilon' \\ \propto_2 \Delta\varepsilon'' \end{bmatrix} \quad (4)$$

where $\propto$ parameters defined the distance between the actual and next value of the permittivity. The convergence criteria are fixed when $\|\Delta\vec{S}\|^2 < 10^{-8}$ and $\propto < 10^{-6}$. In (27), the new value becomes the initial value for next iteration.

Then, a convergence study is carried out to optimize the computing time by limiting the number of modes in each regions. Previous study done in [12] shows that a minimum number of 10 modes is required to accurately model coaxial to coaxial discontinuity and 15 modes for coaxial to circular discontinuity considering the convergence of both the magnitude and phase of reflection and transmission parameters.

REFERENCES

[1] S. Iijima, "Helical microtubules of graphitic carbon," *Nature,* vol. 354, pp. 56-58, November 1991.

[2] M. A. EL Sabbagh and S. M. El-Ghazaly, "Miniaturized carbon nanotube-based RF resonator," *in IEEE MTT-S Int. Microwave Symp. Dig.*, Boston, MA, 7-12 June 2009, pp. 829-832.

[3] J.F. Davis et al., "High-Q mechanical resonator arrays based on carbon nanotubes," *IEEE Conference on Nanotechnology,* San Fransisco, CA, USA, August 2003, pp. 635-638.

[4] M.J. O'Connell, *Carbon Nanotubes Properties and Applications,* Taylor & Francis Group, 2006..

[5] L.F. Chen, C.K. Ong, C.P. Neo, V.V. Varadan and V.K. Varadan, *Microwave Electronics: Measurement and Materials Characterization.* John Wiley & Sons, 2004.

[6] C.A. Grimes, C.E.C. Dickey, C. Mungle, K.G. Ong, and D. Qian, "Effects of purification of the electrical conductivity and complex permittivity of multi wall carbon nanotubes," *J. Appl. Phys.* vol. 90, pp. 4134-4137, October 2001.

[7] L. Liu, L.B. Kong, and S. Matitsine, "Tunable efective permittivity of carbon nanotube composites," *J. Appl. Phys.* vol. 93, 113106, September 2008.

[8] M. EL Sabbagh, S. M. El-Ghazaly, and H. A. Naseem, "Carbon nanotube-based planar transmission lines," *International Microwave Symposium*, Boston, MA, Jun. 2009.

[9] E. Decrossas, M.A. EL Sabbagh, V. Fouad Hanna and S.M. El-Ghazaly, "Broadband characterization of Carbon nanotube networks," *IEEE International Symposium on Electromagnetic Compatibility*, Fort Lauderdale, FL, 27–30 July 2010, pp. 208–211.

[10] N.E. Belhadj-Tahar, and A. Fourrier-Lamer, "Broad-band analysis of a coaxial discontinuity used for dielectric measurements," *IEEE Trans. Microw. Theory Tech*., vol. MTT-34, no. 3, pp. 346-349, March 1986.

[11] T. Itoh, *Numerical Techniques for Microwave and Millimeter-Wave Passive Structures.* John Wiley & Sons, New York, NY, 1989.

[12] E. Decrossas, M.A. EL Sabbagh, V. Fouad Hanna and S.M. El-Ghazaly, "Mode Matching Technique based modeling of coaxial and circular waveguide discontinuities for material characterization purposes," *EuMA, International Journal of Microwave and Wireless Technologies,* accepted for publication.

[13] S. Trabelsi, A.W. Kraszewski, and S.O. Nelson, "Phase-shift ambiguity in microwave dielectric properties measurements," *IEEE Trans. Instrum. Meas.*, vol. 49, no. 1, pp. 56 – 60, Feb. 2000.

[14] M. EL Sabbagh and S. M. El-Ghazaly, "Measurement of dielectric properties of carbon nanotube networks used to build planar transmission lines," *IEEE Int. Symposium Electromagnetic Compatibility*, Aug. 2009.

[15] N.N. Al Moayed, U.A. Khan, M. Obol, S. Gupta, and M.N. Afsar, "Characterization of single- and multi-walled carbon nanotubes at microwave frequencies," *Instrumentation and Measurement Technology Conference,* Warsaw, Poland, 1-3 May 2007.

[16] H. Xu, M. Anlage, L. Hu, and G. Gruner, "Microwave shielding of transparent and conducting single-walled carbon nanotube films," *J. Appl. Phys.* Vol. 90, 183119, May 2007.

[17] D. Stauffer and A. Aharony, *Introduction to Percolation Theory, Taylor an*d Francis, Washington, DC, 1992.

[18] E. Decrossas, M.A. EL Sabbagh, H.A., Naseem, V. Fouad Hanna, and S.M. El-Ghazaly, "Effective permittivity extraction of dielectric nano-powder and nano-composite materials: effects of packing densities and mixture compositions," *IEEE European Microwave Week*, Manchester, UK, October 9-14, 2011.

[19] F. He, S. Lau, H.L. Chan, and J. Fan, "High dielectric permittivity and low percolation threshold in nanocomposites based on poly (vinylidene fluoride) and exfoliated graphite nanoplates," *Adv. Mat.,* no. 21, pp. 710-715, 2009.

[20] S. Link, M.B. Mohamed, and M.A. El-Sayed, "Simulation of the optical Absorption spectra of gold nanorods as a function of their aspect ratio and the effect of the medium dielectric constant," *J. Phys. Chem. B,* 1999, 103,pp. 3073-3077.

Emmanuel Decrossas (S'10) received the B.S. and M.S with honors in engineering science and electrical engineering from the université Pierre et Marie Curie Paris-6, Paris, France in 2004 and 2006 respectively. He is actually pursuing his Ph.D. in electrical engineering in the University of Arkansas, Fayetteville, AR, USA.

In 2004, he joined France Telecom for an internship to develop and update the intranet services. He was an intern in Laboratoire de Génie Eléctrique de Paris (LGEP) in 2005. Mr. Decrossas was a visiting scholar student in 2006 in the University of Tennessee to initiate an international student exchange program and work on reconfigurable MEMS antennas for wireless applications. His research interests include dielectric characterization, computer-aided design of microwave devices, micro/nano-fabrication and nanotechnology to fabricate and model high frequency devices.

Mr. Decrossas is member of the electrical engineering honor society Eta Kappa Nu.

Mahmoud A. EL Sabbagh (S'93–M'02–SM'06) received the B.S. (with honors) and M.S. degrees in electrical engineering from Ain Shams university, Cairo, Egypt, in 1994 and 1997, respectively, and the Ph.D. degree from the University of Maryland, College Park (UMCP), in 2002.

Dr. Sabbagh is holding the position of Professor of Practice in the EECS Department, Syracuse University and also working with Anaren Microwave, Inc. He is cofounder of EMWaveDev where he is involved in the design of ultra-wideband microwave components.

Dr. EL Sabbagh worked at several academic and governmental institutes in Cairo, Canada, and US. His research interests include computer-aided design of microwave devices, microwave filter modeling and design for radar and satellites applications, dielectric characterization, metamaterial, EM theory, and RF Nanotechnology.

Prof. EL Sabbagh is a member of Sigma Xi and he was cited in the 2008–2009 edition of "Who's Who in Science and Engineering."

Victor Fouad Hanna (F'96) received the B.Sc degree (honors) in electronics engineering from Cairo University, Cairo, Egypt in 1965, and the M.Sc. degree in microwave engineering from Alexandria University, Egypt in 1969. He received the D.Sc. degree [Doctorat -Sciences Physiques (doctorat d'Etat)] from l'Institut National Polytechnique (I.N.P.), Toulouse, France in 1975.

Since 1997, he is a professor at the University Pierre et Marie Curie (University of Paris 6) in the electronic department. His current research interests deal with electromagnetic theory, numerical methods, characterization, millimeter-wave transmission lines and bio-electromagnetism.

Prof. Fouad Hanna was selected as recipient of the IEEE third Millenium medal. He was the chairman of the Commission B of the URSI in France from 2001 to March 2004. He was the president of the IEEE France Section during the period 2002-2005. He is a member of the Region 8 IEEE Educational Activities Committee since January 2003 and a chair of this committee for 2004, 2005 and 2006. He is chair of the region 8 Awards and Recognition Committee since January 2007. Prof. Fouad Hanna was an elected member of the IEEE Fellow Committee for the years 2008 and 2009.

Samir M. El-Ghazaly (S'84–M'86–SM'91–F'01) received the B.S and M.S with honors in electronics and communications engineering from Cairo university in 1981 and 1984, respectively and the Ph.D. degree in electrical engineering from the University of Texas at Austin, in 1988.

He is currently the department head of the University of Arkansas, Fayetteville, since 2007.His research interests include RF and microwave circuits and components, microwave and millimeter-wave semiconductor devices, electromagnetic, and numerical techniques applied to MMICs radio-frequency nanotechnology devices.

Prof. El-Ghazaly is a member of Tau Beta Pi, Sigma Xi, and Eta Kappa Nu. He is an elected member of Commissions A and D, URSI. He is a member of the Technical Program Committee for the IEEE Microwave Theory and Techniques Society (IEEE MTT-S) International Microwave Symposium (IMS) since 1991. He is on the Editorial Board of the IEEE TRANSACTIONS ON MICROWAVE THEORY AND TECHNIQUES. He is an elected member of the Administrative Committee of the IEEE MTT-S. He is the editor-in-chief of the IEEE MICROWAVE AND WIRELESS COMPONENTS LETTERS. Prof. El-Ghazaly was the president of the IEEE's Microwave Theory and Techniques Society (MTT-S) in 2010.